Automated classification of coastal defense structures using airborne bathymetric LiDAR

Jan Rhomberg-Kauert[1], Lucas Dammert[1], Gottfried Mandlburger[1], Tomasz Kogut[2], Arkadiusz Tomczak[2] and Małgorzata Jarząbek-Rychard[3]

[1]Department of Geodesy and Geoinformation, TU Wien; 1040 Vienna, Austria
- jan.rhomberg-kauert@geo.tuwien.ac.at, lucas.dammert@geo.tuwien.ac.at, gottfried.mandlburger@geo.tuwien.ac.at
[2] Faculty of Geoengineering and Environmental Protection, Maritime University of Szczecin
- t.kogut@pm.szczecin.pl, a.tomczak@am.szczecin.pl
[3] Institute of Geodesy and Geoinformatics, Wrocław University of Environmental and Life Sciences
- malgorzata.jarzabek-rychard@upwr.edu.pl

Keywords: coastal management, tides, currents, waves, infrastructure, groynes

Abstract

Coastal defense structures, such as breakwaters and groynes are an integral part of coastal engineering. These structures reduce the impact of waves and decrease beach erosion, due to the constant forces to which they are exposed, repeated monitoring and evaluation is vital to the analysis of their structural integrity. However, coastal defense structures are most often located in the turbulent waters of the surf zone, which characteristics pose severe challenges for existing methods. For example, waves pose challenges for image-based analysis, shallow-water limits the efficiency sonar-based measurements, and currents make for hazardous environments for surveying personnel. Here, recent advances in topo-bathymetric LiDAR have improved the ability to map data above and below the water surface within the same survey. In the field of structural engineering, point cloud data is already commonly used, and thus its applications in the monitoring of coastal defense structures present a natural extension of existing structural monitoring methods. Therefore, this study presents an automatic method for the detection of coastal defense structures with topo-bathymetric LiDAR. The surveyed area consists of multiple groynes located along the Polish coast, which were surveyed using an airplane-based topo-bathymetric LiDAR scanner. The presented method then leverages the echo ratio and repeated clustering to automatically extract the groynes from the data. We evaluate the extracted structures in comparison to manually annotated data. The results of this evaluation display a balanced accuracy of 96%, indicating an overall match with the reference data, but showing challenges and improvements for future work.

1. Introduction

Coastal defense structures are a common feature along shorelines, as they protect ports, marinas, and beaches from waves and currents (Diab et al., 2017; Sousa et al., 2022). To achieve this task, many different geometries and dimensions of breakwater structures and groynes have been deployed and tested over time (Falkenrich et al., 2021; Lemos et al., 2020). For breakwater structures, such as tetrapods or rubble mound breakwaters, the monitoring using optical remote sensing methods has been explored in order to analyze changes and degradation of the structures over time (Bueno et al., 2015; Puente et al., 2014). This is of great importance in coastal engineering, as the assessment of structural integrity is vital for the overall functionality of the structures (Shaw et al., 2019; Sousa et al., 2022).

Photogrammetric methods using airborne imaging, in recent years based on unmanned aerial vehicles (UAVs), allow the three-dimensional reconstruction of coastal defense structures and analysis of sediment movements (Helmholz et al., 2023; Shaw et al., 2019; Sousa et al., 2022). Similarly, near-infrared (NIR) LiDAR deployed from UAVs or mounted on a terrestrial laser scanner has been well established to reconstruct coastal defense structures and monitor changes along waterways above the waterline (Shaw et al., 2019; Tschirschwitz et al., 2016). In general, photogrammetry and LiDAR have become a standard tools to assess changes and potential damage in structural engineering (Kaartinen et al., 2022; Lee et al., 2019). For coastal defense structures, the main challenge in data acquisition is that these structures extend below the water surface. This poses challenges for both photogrammetric and NIR LiDAR methods, as photogrammetry faces challenges through turbulent and turbid waters, while NIR is limited to above-water structures (Mandlburger, 2022; Puente et al., 2014; Scott et al., 2016).

Due to the aforementioned challenges, underwater monitoring tools such as remotely operated vehicles (ROVs) equipped with cameras, divers, and multi-beam echo sounders (MBES) have proven useful for analyzing changes in underwater structures (Mandlburger, 2022). Similarly to airborne photogrammetric methods, ROV-based photogrammetric surveys are also limited by turbidity, with the added risk of damage to the vehicle through waves and currents in close proximity to the structures (Francis and Traykovski, 2021; Mandlburger, 2022). These risks extend to all boats and unmanned surface vehicles (USVs), as the surf zone (near shore waters where waves break) poses an increased risk of collision with coastal defense structures. For divers, this translates into highly hazardous environments depending on the surveyed structures and the currents surrounding the surveyed area (Francis and Traykovski, 2021). Boat-based surveys have been shown to overcome such challenges by deploying sonars, where the minimum draft of the boat and the risk of collision close to the breakwater structures can be mitigated (Jost et al., 2025).

Combining both underwater and above water surface data still presents the possibility of misalignment of the dataset and furthermore increases surveying costs, as different systems and possible survey teams are needed (Dammert et al., 2025;

This contribution has been peer-reviewed. The double-blind peer-review was conducted on the basis of the full paper.
https://doi.org/10.5194/isprs-annals-XI-2-2026-595-2026

Mandlburger et al., 2015a; Mandlburger, 2022). This has led to the application of topo-bathymetric LiDAR to map both above and below the water simultaneously (Irish et al., 2016; Mandlburger et al., 2015b). Airborne, in particular airplane-based, bathymetric LiDAR can be used to survey a large area (Mandlburger et al., 2015b) and thus efficiently monitor coastal defense structures in remote places along the coast line. In contrast to a combination of terrestrial LiDAR and MBES, the acquired data does not need to be matched, and through the combined system of topo-bathymetric laser scanners, movements of water surfaces can be taken into account and accurate refraction corrections applied (Mandlburger, 2022).

A challenge that remains across all point-cloud-based datasets is the automatic classification of the data. This is the case for both terrestrial (Lehtomäki et al., 2015; Wang et al., 2019b) and bathymetric LiDAR surveys (Asgharian Pournodrati et al., 2025; Rhomberg-Kauert et al., 2024). Although the classification and segmentation of infrastructure and buildings have seen a wide range of classification algorithms (Che et al., 2019; Özkan et al., 2022), only recently have such methods seen wider applications in maritime infrastructure, specifically breakwater structures and groynes (Arza-García et al., 2024; Pellerin Le Bas et al., 2024; Xu et al., 2022). In contrast to terrestrial landscapes, the lack of large scale annotated datasets and the general challenge of manual annotation of submerged environments limit the classification using machine learning approaches (Pellerin Le Bas et al., 2024; Rhomberg-Kauert et al., 2024). Both supervised and unsupervised classification methods build on the characteristic of the data, which can be used to classify the LiDAR data (Pellerin Le Bas et al., 2024; Rhomberg-Kauert et al., 2024; Xu et al., 2018). Therefore, this study aims to extend such feature-dependent classification methods to wooden coastal defense structures (groynes) in the Polish coastal area of the Baltic Sea.

The groynes along the surveyed Polish coastline consist of wooden pillars, embedded next to each other, forming a rigid structure perpendicular to the coast line. Similarly to breakwater structures, groynes prevent erosion of the coast line and limit sediment movement. As these structures extend from the beach outward, they are located within the shallow and turbulent waters of the surf zone and display the challenges described above. Thus, the study site is well-suited for airborne topo-bathymetric LiDAR.

For the selected study site, this study therefore introduces a new method to classify wooden coastal defense structures through the combination of established components, e.g., echo ratio based classification (Höfle et al., 2012), density-based clustering (Ester et al., 1996) and multi-resolution clustering (Zappia and Oshlack, 2018). The method specifically leverages the linear structure of the groynes and the emergent features of the wood pillar to distinguish the structure from the surrounding coastal waters. While previous work has mostly relied on images or terrestrial LiDAR, the usage of topo-bathymetric LiDAR does allow for a mapping of the coastal defense structure as well as the surrounding costal waters, thus enabling an in-depth analysis and structural monitoring.

In our study, first, the study site and the acquired LiDAR data

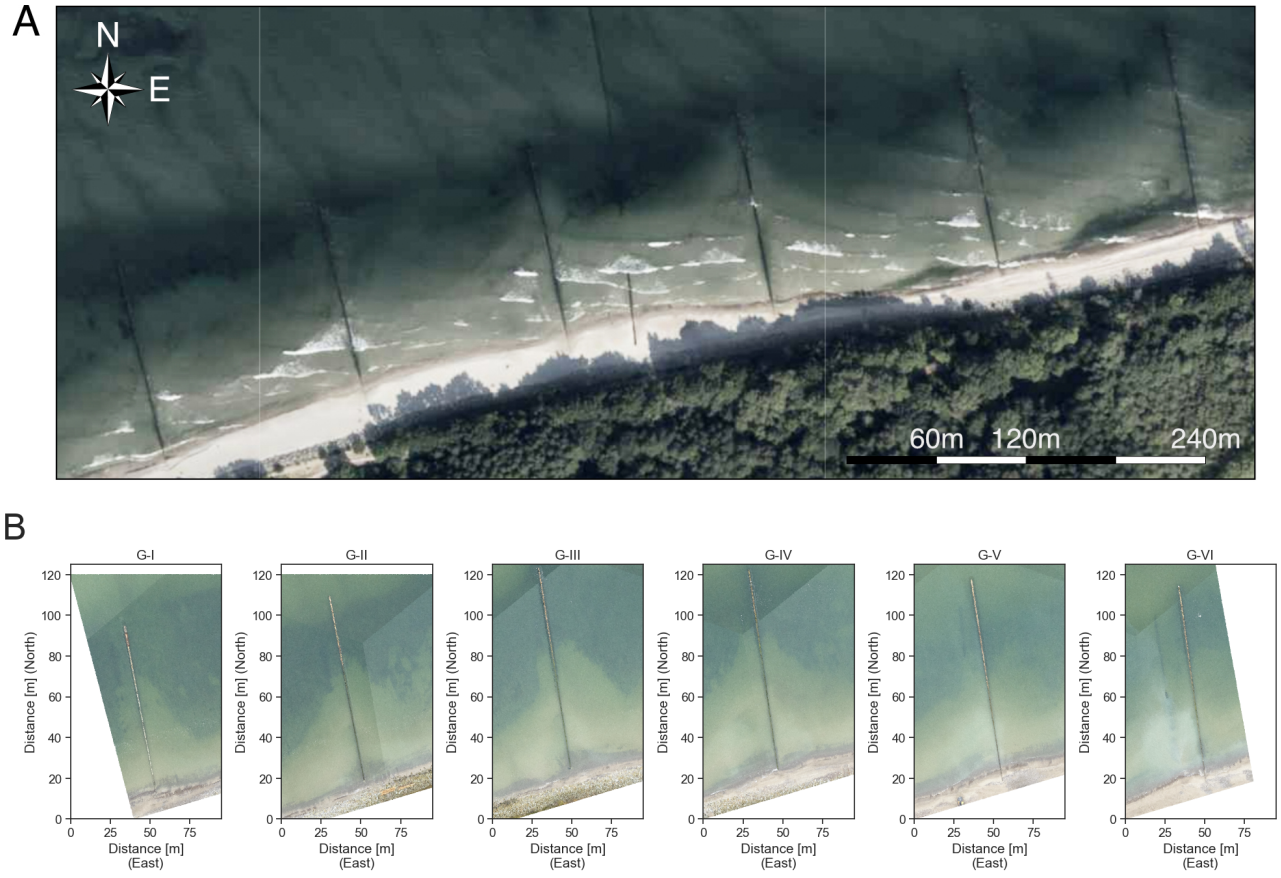

Figure 1. (A) Orthophoto of the study area near Kołobrzeg, Poland, (GUGiK; Head Office of Geodesy and Cartography, 2025) and (B) the six groynes in the area of interest as a top-down-view of the colored point cloud, split into 100 m sections along the coastline.

are introduced (Section 2). Second, the developed automatic detection algorithm of groynes is presented, which divides the coastal area into single groyne sections and, through tiling and classification of each tile, extracts the coastal defense structure from the LiDAR data (Section 3). The automated detection can then be evaluated by comparing against manually annotated data (Section 4). The results are then critically discussed (Section 5) and lastly a conclusion of the gained insight is given (Section 6).

2. Materials

The study site (centered around $54.1921°$N, $15.6155°$E) is located near Kołobrzeg on the Polish coast of the Baltic Sea. There, along the coast, the landscape features repeated groynes, as coastal defense structures (Figure 1). The area of interest was surveyed using an airplane-based *RIEGL* VQ880-GII topo-bathymetric laser scanner. The bathymetric LiDAR system uses a wavelength of $532\,\mathrm{nm}$, with a divergence of the beam of $1.3\,\mathrm{mrad}$ and an average range of $550\,\mathrm{m}$ during the survey. This results in an average footprint diameter of $0.7\,\mathrm{m}$ and a two-dimensional point density of $134\,\mathrm{points/m^2}$ for all combined flight strips. The LiDAR data was processed using online waveform processing (Pfennigbauer et al., 2009) and refraction corrected using RiHYDRO. Lastly, the generated point cloud is exported to WGS84/UTM33N.

During measurement, the costal waters were mostly calm with minimal waves and overall stable measurement conditions with the laser scanner capable of capturing a depth of up to $6\,\mathrm{m}$. Although here it should be noted that due to the typical movement of coastal water in the shallower regions (less than $1\,\mathrm{m}$), there was noticeable sediment movement present in the water column.

To reduce computational time, the general survey area is furthermore cut out manually to minimize the extent, roughly capturing the groynes and beach along the coast line (Figure 1 A). This yields the main input dataset of the method, which can now be manually annotated for the evaluation of the method. For the annotation, the colorization of the point cloud and the linear structures were leveraged and each groyne was annotated using polylines to separate the groynes from the rest of the data. All separated groynes were then assigned to the same class (one), with the rest of the point cloud assigned zero.

3. Method

The automated detection of coastal defense structures is divided into tile-wise classification and macro-extraction (Figure 2). After the LiDAR data is split into single groyne section, these sections can be tiled. Then, for each tile, the tile-wise classification assesses whether it contains a section of the groyne, and if so labels it as such. In the macro-extraction these tiles are then combined to extract the complete groyne. This extraction is done by a secondary clustering step, which detects the largest connected section of the groyne. For the extracted section, a line can be fitted, allowing to leverage the linear geometry of the groynes to capture all segments across all tiles (line-propagation). To avoid a bias through the parameter selection during the tiling, this is done for multiple set of tile parameters, and thus the final step of the method combines all potential groynes from the differently parameterized macro-extractions into a single labeling (multi-resolution consensus).

Most parameters of the study were empirically selected based on the measurement conditions, human oversight during the development, and the distinct structural features of the wooden coastal defense structures surveyed (Table **??**. Although the multi-resolution consensus step overcomes the problem of tile size section, the other parameters were chosen based on the emergent structure of the groynes (height threshold), the ability to detect the structure (echo ratio radius) and the general size of the clusters for each tile (cluster size limit). That these assumptions are well suited for the area survey is later outlined in

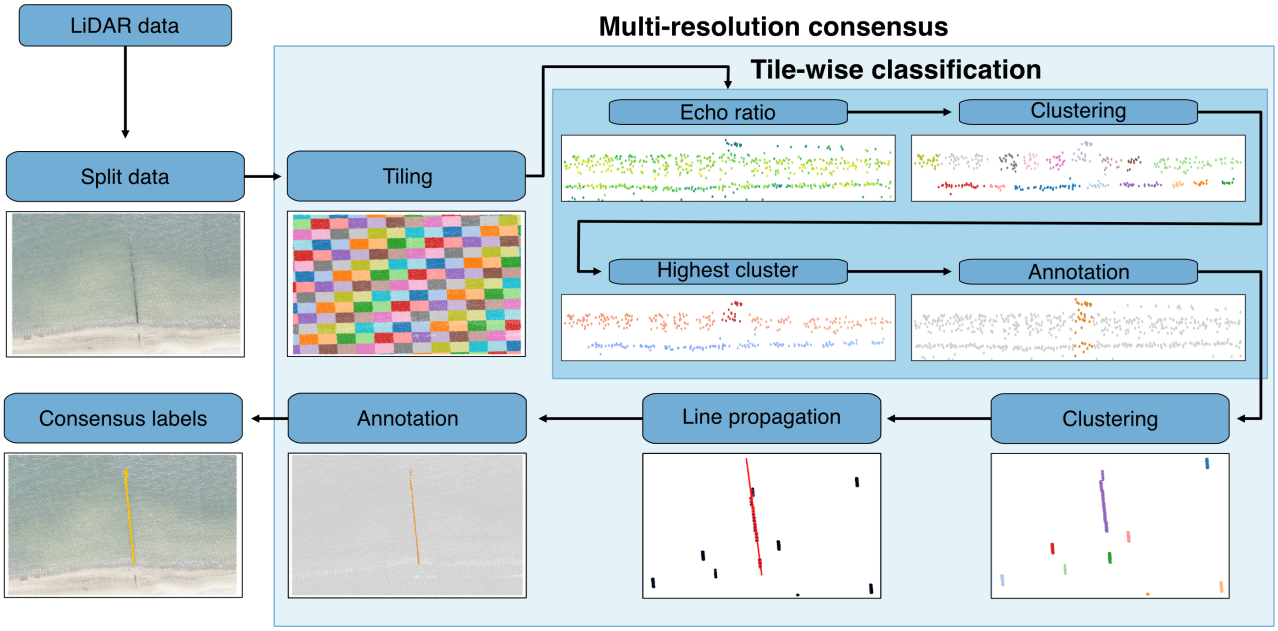

Figure 2. Flow-chart of each step in the automatic coastal defense structure detection, with the two main parts of the method marked by the blue boxes (Multi-resolution consensus and tile-wise classification). In the tile-wise classification the plots show cross sections of the the tiles, while the other plots outside the darker blue box always show north-east projections of the point cloud.

This contribution has been peer-reviewed. The double-blind peer-review was conducted on the basis of the full paper.
https://doi.org/10.5194/isprs-annals-XI-2-2026-595-2026

Section 4.3. In general, the analysis parameters are described in Table 1.

Parameters employed		Values
Echo ratio radius	[m]	0.2
Height threshold	[m]	0.1
Cluster size limit	[%]	20
Tile size (multi-resolution consensus)	[m × m]	$\{2, 4, 5, 6, 8, 10\} \times \{2, 4, 5, 6, 8, 10\}$
min_cluster_size (HDBSCAN)	[-]	10

Table 1. Fixed parameters of the costal defense structure classification.

3.1 Data separation

To extract the groynes from the surveyed coastal area, the data is first split into sections consisting of single groynes, either manually set or provided through national databases. As these structures occur in consistent distances to each other, the separation is performed by selecting an approximate distance threshold, in this case $100\,\mathrm{m}$. The resulting sections each contain a single groyne and serve as the input for tiling. Then, the method groups the point cloud into tiles of a given width and length. Each tile must have a minimum number of 100 points to avoid artifacts based on low density in the processing workflow. Thus, the point cloud is split into equal tiles, with a separated class of low-density tiles, which is disregarded in the further processing, focusing only on tiles with sufficient point density.

3.2 Tile-wise classification

The backbone of the method consists of the tile-wise classification. There, the structure of the groynes are leveraged to enable automatic detection, as the structures extend above the water surface, and thus have a different point density and distribution compared to the rest of the open-water point cloud in the x-z-cross section. This is leveraged to separate the pillars of the groyne by clustering, and thus extract sections of the groyne for each tile.

3.2.1 Echo ratio and clustering The visible difference of the groynes and open water is translated for the automatic detection using the echo ratio (Equation 1). Let $p \in \mathcal{P}$ be a point within the LiDAR point cloud. Then the two-dimensional neighborhood of radius $r \in \mathbb{R}_{>0}$ is defined as $\mathcal{N}_r^2(p)$, where $|\mathcal{N}_r^2(p)| = n_{2d}$. Analogously, the three-dimensional neighborhood of p is defined as $\mathcal{N}_r^3(p)$ with $|\mathcal{N}_r^3(p)| = n_{3d}$. The echo ratio (ER), is thus defined as the fraction of the point within the three-dimensional neighborhood divided by the point within the two-dimensional neighborhood.

$$\mathrm{ER} = \frac{|\mathcal{N}_r^3(p)|}{|\mathcal{N}_r^2(p)|} = \frac{n_{3d}}{n_{2d}} \tag{1}$$

The groynes in the survey area are less than $0.5\,\mathrm{m}$ in width and therefore a neighborhood radius of $0.10\,\mathrm{m}$ is selected to adequately capture the difference in point density of the wooden pillar versus the costal area. In combination with the perpendicular construction of the structures w.r.t. to the coastline, a three-dimensional dataset is constructed using the two-dimensional projection of the groynes along the coastline (height and distance along the coast) combined with the echo ratio. This dataset is then be clustered in the next step using a hierarchical clustering algorithm, in this case HDBSCAN (Pedregosa et al., 2011). To reduce false-positive annotations, this step is refined with two thresholds. First, the height of the cluster in the cross section (height of the center of the cluster in Figure 2) must be at least $20\,\mathrm{cm}$, which in the selected coordinate system translates to the center being above the water line. Second, the cluster must contain less than 20% of the point cloud, to avoid outlier clusters being mistaken for coastal defense structures, especially as the detected clusters only correspond to the uppermost part of the groyne.

3.2.2 Highest cluster selection For each cluster generated using HDBSCAN, the average height of the cluster can be determined by calculating the mean height value of all points within the cluster. This results in varying cluster heights regardless of whether the cluster belongs to the water surface, bottom, or coastal defense structure. Here, the highest cluster corresponds to the top part of the groynes, as the wooden pillars of the structure emerge from the water surfaces. This cluster is then extended to the entire pillar through the known constructions of the groyne (vertical pillars perpendicular to the coastline). First, the center of the cluster is determined, and then a radius from the center of the cluster to the outermost point of the cluster is determined. As the groynes represent a symmetrical structure when looking at each tile (cross section), the cluster should consist of the most left and right points of each individual section. Thus, to annotate the entire pillar, the center of the cluster can then be used to annotate all points in the cross section left and right of the cluster center within the maximal radius of the coastal defense structures.

3.3 Macro-extraction and multi-resolution consensus

To link the detected groyne sections of each tile, the method extends the tile-wise classification towards the single groyne section. For this, all groyne segments are clustered to extract the longest segment. The longest extracted segment can then be used to fit a line to the structure, that extends the largest cluster to capture the whole structure. Lastly, the process can be repeated for multiple resolutions, which are then merged to find the consensus across all input tiling resolutions.

3.3.1 Macro clustering and line propagation To separate true groyne sections from outliers produced by the tile-wise classification. All potential groyne sections undergo a second round of clustering to extract the longest segment, which minimizes the chance of false classification, as the consecutive tiles should be part of the same coastal defense structure. For this again, HDBSCAN is used with a minimum cluster size of 10 points (Pedregosa et al., 2011). The longest connected component then encompasses a section of the groyne.

To extend this section to the entire structure, a line is fitted to the section using least squares fitting (Virtanen et al., 2020). The fitted line should align within all clusters that are potentially part of the structure but were not detected by the clustering due to gaps in the data. Therefore, the line limits are set to the upper and lower limits of the distance along the coast and to account for the underestimation (along the coastline), extended by $\pm 10\,\mathrm{m}$. Along this line, all clusters of the second clustering are examined if the minimum distance of the cluster to the line is less than $0.15\,\mathrm{m}$ and if so, the cluster is added to the component. In addition, to bridge potential gaps in the data, the upper and lower limit of the distance along the coast are determined for all selected clusters after the previous step. For all points

with a proximity of $0.15\,\mathrm{m}$ to the extended line, they are additionally classified as coastal defense structures, if they have not already been classified as such.

3.3.2 Annotation To avoid the problem of parameter selection in the tiling, the method introduces a final step to merge classification labels from multiple resolutions and thus establish a consensus clustering approach. Depending on the input parameters, the labels produced after line propagation could be used as final labels. However, these labels would potentially lead to revisiting of the tiling to achieve an optimal tiling resolution for the selected dataset, where tiling parameters could furthermore differ for each groyne, depending on the integrity and extent of the structure. Therefore, the tiling is run for all combinations of the tile parameters (width and length) of the set $\{2\,\mathrm{m}, 4\,\mathrm{m}, 5\,\mathrm{m}, 6\,\mathrm{m}, 8\,\mathrm{m}, 10\,\mathrm{m}\}$. This produces 36 independent classifications of the single-groyne section. As the detected structure within each section should be the groyne, the point-wise labels can be compared, and if the coastal defense structures labels match for three or more classifications the label is assigned to the point.

3.4 Evaluation metrics

To evaluate the automatic detection of the groynes, we use evaluation metrics precision, recall, F-beta, and balanced accuracy (Brodersen et al., 2010; Towards data science, 2026) as implemented in *scikit-learn* (Pedregosa et al., 2011). For the F-beta score, in particular, a beta of 2 was selected due to the asymmetric nature of the point-cloud labels. Let the prediction be divided into positive P and negative N. This results in four classes: True positive TP, true negative TN, false positive FP, and false negative FN. With this, the evaluation metrics are defined as

$$\begin{aligned}
\text{Precision} &= \frac{TP}{TP+FP}, \\
\text{Recall} &= \frac{TP}{TP+FN}, \\
F_\beta &= \frac{(1+\beta^2)\cdot TP}{(1+\beta^2)\cdot TP + FP + \beta^2 FN}, \\
\text{Balanced accuracy} &= \frac{1}{2}\left(\frac{TP}{TP+FN} + \frac{TN}{TN+FP}\right).
\end{aligned}$$

These have been selected to give an overall assessment of the performance of the method. In addition, we also show confusion matrices (Figure 4B) to give more specific insight into the true and false positives and negatives, as the groynes are long but thin structures compared to the surveyed coastline and therefore evaluation faces a distinct challenge of highly unbalanced labels. Thus, the selected metrics aim to avoid bias based on this inhomogeneity of labels. Nevertheless, the asymmetric distribution of labels has to be kept in mind during the evaluation.

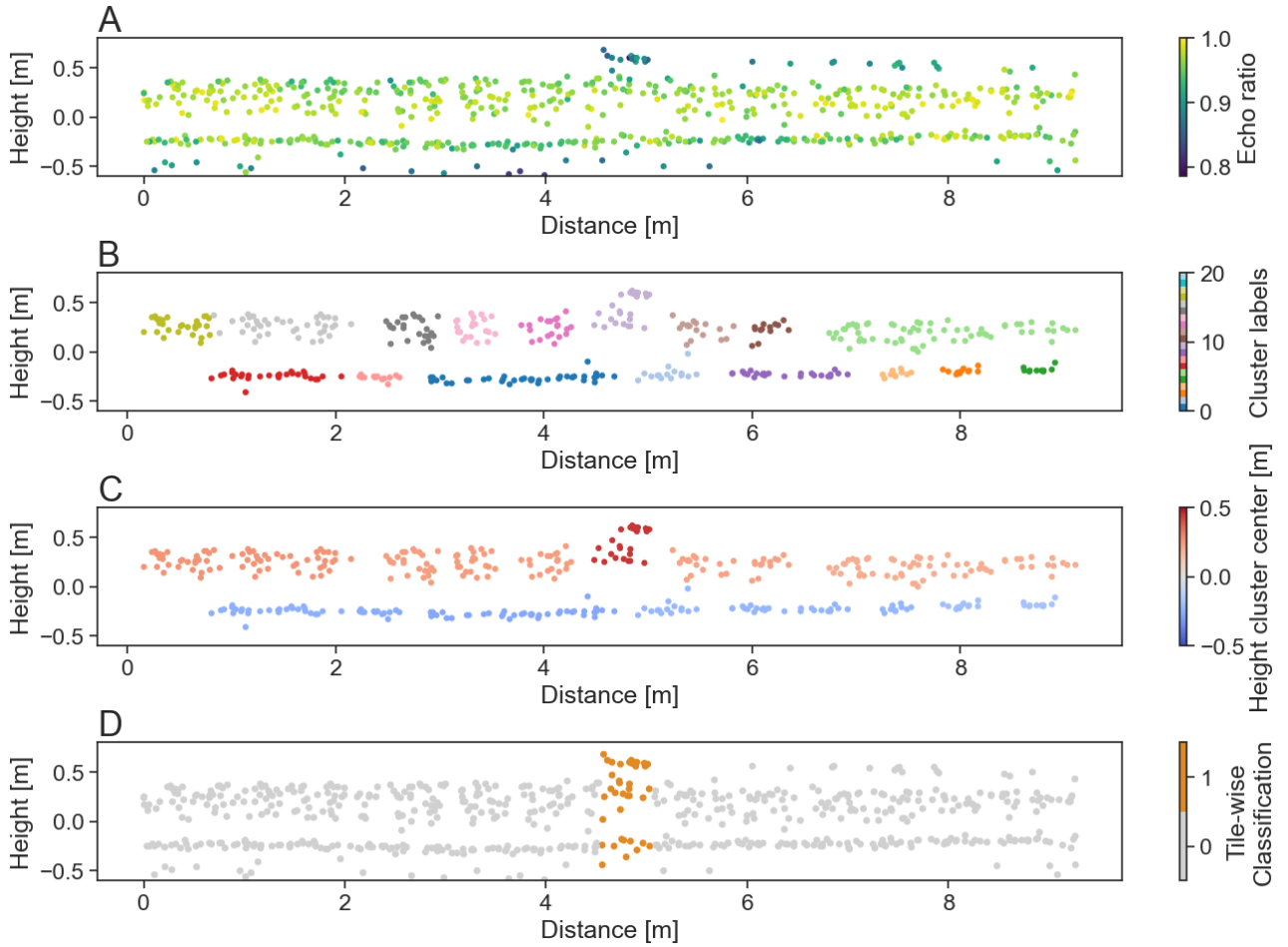

Figure 3. (A) Cross section of a single tile colored by the echo ratio, were the x-axis matches the coastline. (B) The cluster labels of the tile-wise clustering for the three dimensional dataset shown in the previous panel. (C) The extracted mean height for each cluster. (D) The tile-wise classification of the coastal defense structures.

3.5 Sensitivity analysis

To finally evaluate the chosen parameters and provide evidence that these parameters are well suited for the surveyed costal landscape, this section presents a sensitivity analysis of the three main parameters. These parameters are the *height threshold*, the *echo ratio radius*, and the *cluster size limit* (Table 1). For the three parameters, the following ranges of parameters were selected (Table 2). For each combination of these ranges with the selected parameters shown in Table 1 the entire workflow is computed, and thus the results can later be compared to evaluate the sensitivity of the individual parameters.

Parameters employed	Values
Echo ratio radius [m]	$\{0.05, 0.1, 0.15, 0.2, 0.25\}$
Height threshold [m]	$\{0.05, 0.1, 0.15, 0.2, 0.3\}$
Cluster size limit [%]	$\{0.1, 0.15, 0.2, 0.25, 0.3\}$

Table 2. Variation of parameters for the sensitivity analysis.

4. Results

The results are split into the tile-wise classification, where the individual results of each step of the classification process are presented as they are applied to a tile, and the overall evaluation of the consensus labels for each single groyne section.

4.1 Tile-wise classification

The initial feature space of a tile that contains a section of the groyne is shown in Figure 3 A. There, the characteristics of the point cloud can be seen, as the echo ratio is lower for the pillars that extend above the water surface, in comparison to the water surface and bottom. The next step of the method is shown in Figure 3 B, displaying the different clusters of the initial feature space. The average height for each cluster is then computed (Figure 3 C), where the pillars of the groyne that extend above the water surface show an expected higher average height compared to the rest of the point cloud. This increased average height allows for the outlined separation of the groyne from the rest of the point cloud and the classification of the coastal defense structure for the presented tile (Figure 3 D).

4.2 Consensus labels

From the tile-wise detection, the results can be extended through the line propagation and consensus clustering to classify the groynes within each single groyne section. For each section, the consensus labels show a general visual alignment with the colored point cloud (Figure 4 A). For G-I, G-III, G-IV and G-VI (Figure 4 A) the consensus labels show no deviations from the structure and display neither an overestimation nor an underestimation of the coastal defense structure. For G-II an underestimation toward the sea can be seen, where the coastal defense structures have not been completely detected. Furthermore, for G-V also a slight overestimation into the coast can

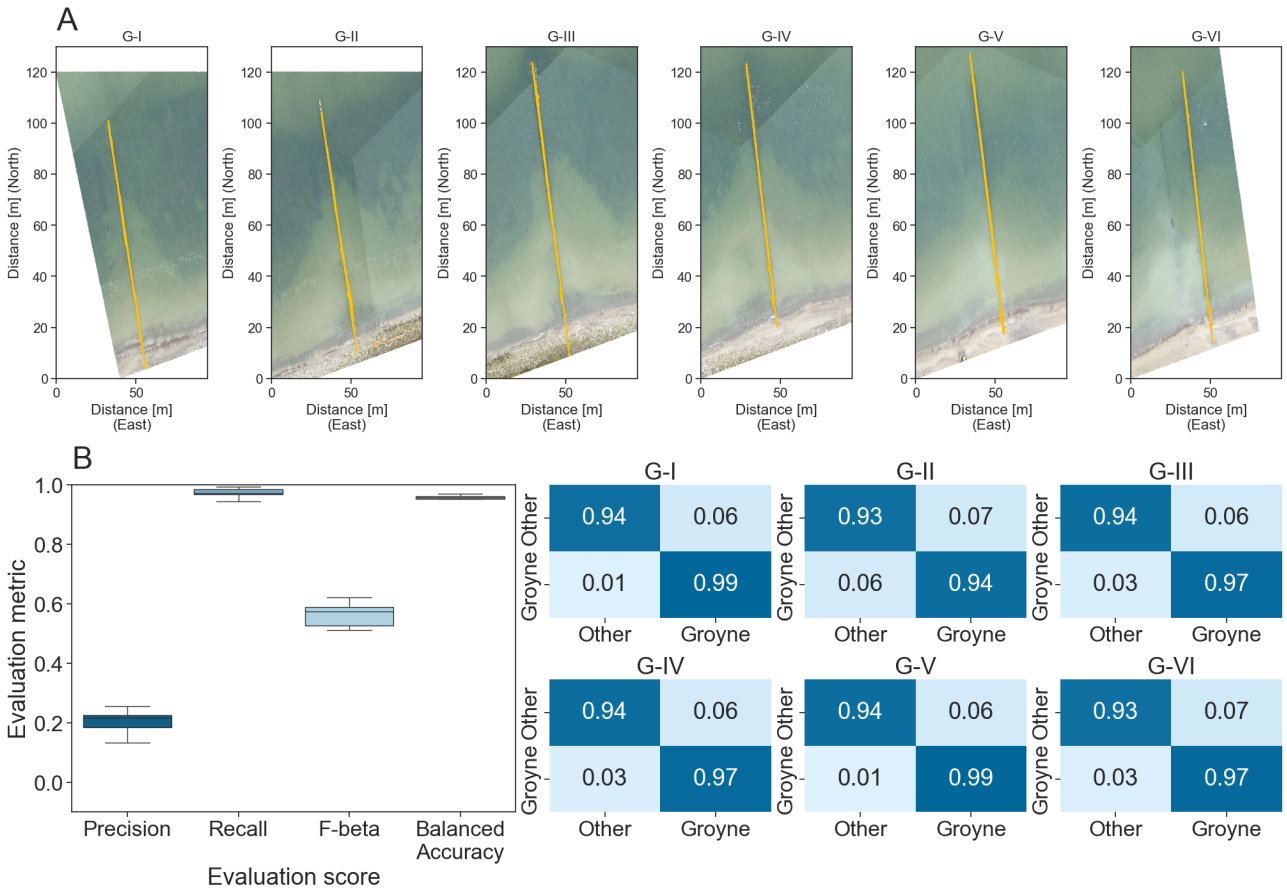

Figure 4. (A) The six groynes shown in Figure 1 B with the consensus labels of the automatic classification in yellow. (B) Quantitative evaluation of the annotated groynes and the consensus labels. On the left a box plot of the evaluation metric results and on the right the confusion matrix for each groyne.

be seen where the consensus labels extend further inland than the annoated data. Nevertheless, none of the sections display outliers, where the consensus labels are not connected to the groyne.

To contextualize the results further, here it has to be noted that the labels align well based on the human annotation, and thus the visibility within the colored point cloud, i.e. the emergent pillars. This puts a general limit to the detection and evaluation, as non-emergence or not directly visible parts of the costal defense structure can not be accounted for. Therefore, the method visually aligns well with human annotation, but for more rigorous evaluation an independent dataset would be required that does not depend on visibility within the point cloud intersect, e.g. side scan sonar.

The quantitative evaluation shows a similar result of the general alignment. The confusion matrices that matched the visual coverage of the consensus labels and the groynes for each section (Figure 4) show values of 0.94 to 0.99 true positives for the groyne class. For the evaluation metrics, the results are not as clear, as there the high imbalance of the two classes influences the scores, and thus the results do not show a consent across all metrics. Recall and balanced accuracy show high scores, with results in agreement and exceeding the scores of the confusion matrices. There, the mean recall is 0.97 and the mean balanced accuracy is 0.96. However, the precision displays overall low scores with a mean value of 0.20 that does not align with the confusion matrices, indicating potential challenges due to the strongly asymmetric distribution of labels. The F-beta score is between precision and recall with a mean value of 0.55, as expected by definition, while the performance is still underestimating the results compared to the confusion matrices.

4.3 Sensitivity analysis

The sensitivity analysis of the parameters used in the study area classification displays that the parameter most prone to deviations in the results is the echo ratio radius (Figure 5). In contrast, the height threshold and the cluster size parameter do not show significant deviations in the evaluation metrics (Figure 5). Furthermore, the sensitivity analysis shows that for the overall low precision score the input parameters do not have a significant effect, while for the other metrics a smaller echo ratio radius improves the final results.

That the echo ratio is the most sensitive parameter is strongly linked to the method itself. As the echo ratio is essential in the classification and visually corresponds to the emergent structure of the groynes, this parameter is closely linked to the detection of the emergent pillar, which builds the backbone for the classification.

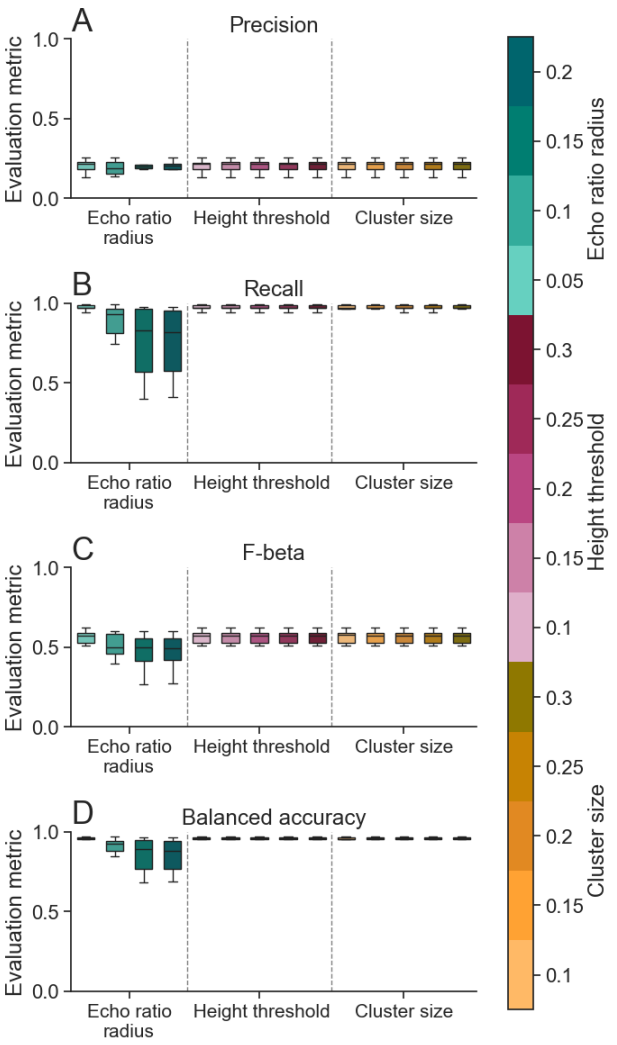

Figure 5. Box plots evaluation metrics split by the variation of the classification parameters. For each input parameter variation the other parameters are kept as shown in Table 1. (Green) Variation of the echo ratio parameter. (Pink) Variation of the height threshold. (Orange) Variation of the cluster size parameter.

5. Discussion

Although little research exists on the automatic detection of coastal defense structures, the challenges in the detection and evaluation of bathymetric LiDAR classification for a multitude of structures are a common topic. The challenges and potential for future work are discussed in this section, both with regard to coastal defense structures and bathymetric LiDAR in general.

5.1 Data annotation and metric selection

The annotation of point cloud data is a challenge in all fields of remote sensing, as the task of manually labeling the data is often time-consuming and prone to subjectivity, depending on the annotator (Pellerin Le Bas et al., 2024; Rhomberg-Kauert et al., 2024). This extends to the annotation of groynes structures in a similar manner, as the surf zone creates additional noise in the data due to uneven water surfaces (Roshandel et al., 2021) and particles in the water column leading to false echoes, which is even more challenging for the annotator compared to less noisy data, e.g. terrestrial LiDAR. Therefore, manual annotation in coastal zones has proven difficult. Additional information, e.g. color information, is especially helpful in these situations. Furthermore, the difficult distinction between the groynes and the turbulent water surface can lead to unknown discrepancies within the results, as false positives and negatives can occur during labeling, which propagate unknowingly throughout the evaluation.

An additional factor is the highly imbalanced distribution of the classes; due to the thin and long structure of the groynes, the results are not constant across all metrics and do not necessarily match the confusion matrices. This is caused by the relatively few points of the coastal defense structures compared

to the surrounding area, leading to a bias in the metrics (King and Zeng, 2001), where the results of the different metrics may reflect more about the label distribution than the performance (Jeni et al., 2013). This can already be seen as a discrepancy between precision and recall. Thus, it limits the spectrum of evaluation metrics applicable to the data. More sophisticated metrics could prove useful in future work together with a more detailed selection of the groynes within the point cloud.

5.2 Parameter selection and supervision

A different challenge for all clustering-based classifications is the selection of appropriate parameters for the dataset (Li et al., 2021; Wang et al., 2019a; Zappia and Oshlack, 2018). This leads to semi-automated workflows, where re-runs of data cost both human and computational resources. Other fields of research have sought to overcome such challenges by applying automated hyperparameter tuning (Fan et al., 2020) or consensus clustering (Lancichinetti and Fortunato, 2012; Virshup et al., 2020), similar to the last step of the workflow presented in our study. However, for consensus clustering approaches, an initial set of parameters must be selected. The presented method had an input of 36 pairs of length and width parameters. Through extended analysis, this number could potentially be reduced to avoid redundant pairs that result in no added information. Such a reduction would improve the overall efficiency.

For the parameter selection of groyne classification, the biggest challenge is the thin and long structure of the groynes. When the tiling divides the coastal defense structures along the main axis, the structure emerging from the water surface might not be distinguishable from noise, as too few points could lead to a classification as outliers or become indistinguishable from the turbulent water surface. Therefore, the multi-resolution approach not only offers added stability for the method but decreases computational efficiency for calm waters or ideal tiling. Regarding the parameters selected themselves (Table 1), the sensitivity analysis displays that the radius of the echo ratio strongly influences the results (Figure 5). In contrast, the other parameters do not show a high degree of sensitivity to small changes. However, future work should explore this to a more rigorous extent and potentially overcome such challenges by expanding the consensus approach, although this would come at the cost of more computational resources.

5.3 Limitations and potential improvements

A major constraint of our method is the differentiation between the water surface and the non-submerged part of the coastal defense structure. As groynes often do not extend far from the water surface, turbulent waters and waves can limit the data quality of bathymetric LiDAR (Roshandel et al., 2021). Furthermore, for monitoring the degradation of coastal defense structures, the non-submerged part of the groyne can be damaged over time and thus become more difficult to detect in LiDAR data (Rad and Scraggs, 2019; Tschirschwitz et al., 2016). Therefore, currently the method is only capable of detecting intact coastal defense structures. In cases where the method cannot detect coastal defense structures even though they should be present, this could potentially indicate degradation. However, this remains a subject for future research.

Improvements towards a more robust detection of intact or impaired coastal defense structures could be the incorporation of color information from aerial images. The presented method did not incorporate them because bathymetric LiDAR data is often not colored, and thus the method remains more general. A different approach could also be the increase of spatial resolution, e.g. by utilizing helicopters or UAVs as the surveying platforms, which, however, limits the efficiency of the data acquisition. Thus, the method presents a suitable workflow for automatic detection, but more testing and comparison with different datasets is needed to draw a final conclusion on the applicability of bathymetric LiDAR to monitor coastal defense structures.

6. Conclusion

The presented automatic classification of coastal defense structures uses a consensus clustering approach to extract groyes from the surveyed coastal waters. The core of the method is built around detection of groyne pillars in cross-sections of the point cloud, where the x and z coordinates together with the echo ratio are able to distinguish the emergent structure of the groyne from the aquatic landscape. In the selected study site of the Baltic Sea, the method is capable of detecting groynes with a true positive rate of 0.94-0.99 compared to manual annotations. This enables potential structural monitoring without exposing surveying personal or equipment to the dangers of the surf zone, while simultaneous increasing efficiency and decreasing surveying costs. Furthermore, future work should examine the differences between UAV-based and airborne (airplane- or helicopter-based) bathymetric LiDAR for the monitoring of coastal defense structures and incorporate a second, presumably acoustic, dataset for validation and potential structural failure detection. In conclusion, the presented workflow presents a novel approach to automated LiDAR-based classification of coastal defenses in an under-researched area. Applied to the surveyed coastline, the method achieved strong performance, accurately delineating groynes with a mean balanced accuracy of 96%.

References

Arza-García, M., Gonçalves, J. A., Ferreira Pinto, V., Bastos, G., 2024. On-Site Stability Assessment of Rubble Mound Breakwaters Using Unmanned Aerial Vehicle-Based Photogrammetry and Random Sample Consensus. *Remote Sensing*, 16(2), 331.

Asgharian Pournodrati, L., Baba, M. M., Gangelhoff, J., Sörgel, U., 2025. Multi-scale Transformer-based classification of bathymetric LiDAR data in shallow water environments. *The International Archives of the Photogrammetry, Remote Sensing and Spatial Information Sciences*, 48, 1–6.

Brodersen, K. H., Ong, C. S., Stephan, K. E., Buhmann, J. M., 2010. The balanced accuracy and its posterior distribution. *2010 20th International Conference on Pattern Recognition*, 3121–3124.

Bueno, M., Díaz-Vilariño, L., González-Jorge, H., Martínez-Sánchez, J., Arias, P., 2015. AUTOMATIC MODELLING OF RUBBLE MOUND BREAKWATERS FROM LIDAR DATA. *The International Archives of the Photogrammetry, Remote Sensing and Spatial Information Sciences*, XL-3/W3, 9–13.

Che, E., Jung, J., Olsen, M. J., 2019. Object Recognition, Segmentation, and Classification of Mobile Laser Scanning Point Clouds: A State of the Art Review. *Sensors*, 19(4), 810.

Dammert, L., Pöppl, F., Rhomberg-Kauert, J., Thalmann, T., Monetti, D., Neuner, H.-B., Mandlburger, G., 2025. Leveraging robotic total stations and multi-sensor adjustment for accurate multibeam bathymetry. *The International Hydrographic Review*, 31(2), 44–62.

Diab, H., Younes, R., Lafon, P., 2017. Survey of research on the optimal design of sea harbours. *International Journal of Naval Architecture and Ocean Engineering*, 9(4), 460–472.

Ester, M., Kriegel, H.-P., Sander, J., Xu, X., 1996. A density-based algorithm for discovering clusters in large spatial databases with noise. *Proceedings of the Second International Conference on Knowledge Discovery and Data Mining*, KDD'96, AAAI Press, 226–231.

Falkenrich, P., Wilson, J., Nistor, I., Goseberg, N., Cornett, A., Mohammadian, A., 2021. Nature-Based Coastal Protection by Large Woody Debris as Compared to Seawalls: A Physical Model Study of Beach Morphology and Wave Reflection. *Water*, 13(15), 2020.

Fan, X., Yue, Y., Sarkar, P., Wang, Y. R., 2020. On hyperparameter tuning in general clustering problemsm. *International conference on machine learning*, PMLR, 2996–3007.

Francis, H., Traykovski, P., 2021. Development of a highly portable unmanned surface vehicle for surf zone bathymetric surveying. *Journal of Coastal Research*, 37(5), 933–945.

GUGiK; Head Office of Geodesy and Cartography, G., 2025. Orthoimagery. https://mapy.geoportal.gov.pl/imap/Imgp$_2$.$html(Accessed$: $2025-09-01).GeoportalPoland.$

Helmholz, P., Boyle, L., Tily-Laurie, B., May, D., Singh, G., Hogben, J., Ren, Y., Li, Q., Belton, D., Khaksar, S. et al., 2023. DETECTION OF BREAKWATER FAILURE MODES FROM PHOTOGRAMMETRIC DERIVED POINT CLOUDS–A CASE STUDY FOR BUNBURY PORT, WESTERN AUSTRALIA. *ICTACT Journal on Soft Computing*, 13(3).

Höfle, B., Hollaus, M., Hagenauer, J., 2012. Urban vegetation detection using radiometrically calibrated small-footprint full-waveform airborne LiDAR data. *ISPRS Journal of photogrammetry and remote sensing*, 67, 134–147.

Irish, J. L., McClung, J., Lillycrop, W. J., 2016. Airborne lidar bathymetry: the SHOALS system.

Jeni, L. A., Cohn, J. F., De La Torre, F., 2013. Facing imbalanced data–recommendations for the use of performance metrics. *2013 Humaine association conference on affective computing and intelligent interaction*, IEEE, 245–251.

Jost, B., Holste, K., Hesse, C., 2025. Digital twins for the sustainable maintenance of ageing waterway infrastructure. *The International Archives of the Photogrammetry, Remote Sensing and Spatial Information Sciences*, XLVIII-2/W10-2025, 147–153.

Kaartinen, E., Dunphy, K., Sadhu, A., 2022. LiDAR-Based Structural Health Monitoring: Applications in Civil Infrastructure Systems. *Sensors*, 22(12), 4610.

King, G., Zeng, L., 2001. Logistic Regression in Rare Events Data. *Political Analysis*, 9, 137–163.

Lancichinetti, A., Fortunato, S., 2012. Consensus clustering in complex networks. *Scientific reports*, 2(1), 336.

Lee, J., Lee, K., Lee, S., Lee, Y., Sim, S., 2019. Long-term displacement measurement of bridges using a LiDAR system. *Structural Control and Health Monitoring*, 26(10).

Lehtomäki, M., Jaakkola, A., Hyyppä, J., Lampinen, J., Kaartinen, H., Kukko, A., Puttonen, E., Hyyppä, H., 2015. Object classification and recognition from mobile laser scanning point clouds in a road environment. *IEEE Transactions on Geoscience and Remote Sensing*, 54(2), 1226–1239.

Lemos, R., Peña, E., Santos, J., Sande, J., Figuero, A., Alvarellos, A., Laiño, E., Reis, M. T., Fortes, C. J., Kerpe, N. B. et al., 2020. 3D surveynmodelling for damage assessment in rubble-mound breakwaters under oblique wave incidence. *Italian journal of engineering geology and environment*, 73–85.

Li, C., Gao, F., Han, X., Zhang, B., 2021. A New Density-Based Clustering Method Considering Spatial Distribution of Lidar Point Cloud for Object Detection of Autonomous Driving. *Electronics*, 10(16), 2005.

Mandlburger, G., 2022. A review of active and passive optical methods in hydrography. *The International Hydrographic Review*, 8–52.

Mandlburger, G., Hauer, C., Wieser, M., Pfeifer, N., 2015a. Topo-bathymetric LiDAR for monitoring river morphodynamics and instream habitats—A case study at the Pielach River. *Remote Sensing*, 7(5), 6160–6195.

Mandlburger, G., Hauer, C., Wieser, M., Pfeifer, N., 2015b. Topo-Bathymetric LiDAR for Monitoring River Morphodynamics and Instream Habitats—A Case Study at the Pielach River. *Remote Sensing*, 7(5), 6160–6195.

Özkan, T., Pfeifer, N., Styhler-Aydın, G., Hochreiner, G., Herbig, U., Döring-Williams, M., 2022. Historic Timber Roof Structure Reconstruction through Automated Analysis of Point Clouds. *Journal of Imaging*, 8(1), 10.

Pedregosa, F., Varoquaux, G., Gramfort, A., Michel, V., Thirion, B., Grisel, O., Blondel, M., Prettenhofer, P., Weiss, R., Dubourg, V., Vanderplas, J., Passos, A., Cournapeau, D., Brucher, M., Perrot, M., Duchesnay, E., 2011. Scikit-learn: Machine Learning in Python. *Journal of Machine Learning Research*, 12, 2825–2830.

Pellerin Le Bas, X., Froideval, L., Mouko, A., Conessa, C., Benoit, L., Perez, L., 2024. A New Open-Source Software to Help Design Models for Automatic 3D Point Cloud Classification in Coastal Studies. *Remote Sensing*, 16(16), 2891.

Pfennigbauer, M., Rieger, P., Studnicka, N., Ullrich, A., 2009. Detection of concealed objects with a mobile laser scanning system. *Laser Radar Technology and Applications XIV*, 7323, SPIE, 51–59.

Puente, I., Sande, J., González-Jorge, H., Peña-González, E., Maciñeira, E., Martínez-Sánchez, J., Arias, P., 2014. Novel image analysis approach to the terrestrial LiDAR monitoring of damage in rubble mound breakwaters. *Ocean Engineering*, 91, 273–280.

Rad, M., Scraggs, C., 2019. Monitoring and maintenance of rock armour groynes-case study: Inspecting rock armoured groynes in gold coast. *Australasian Coasts and Ports 2019 Conference: Future directions from 40 [degrees] S and beyond, Hobart, 10-13 September 2019: Future directions from 40 [degrees] S and beyond, Hobart, 10-13 September 2019*, Engineers Australia Hobart, 965–971.

Rhomberg-Kauert, J., Dammert, L., Grömer, M., Pfennigbauer, M., Mandlburger, G., 2024. Macrophyte detection with bathymetric LiDAR – Applications of high-dimensional data analysis for submerged ecosystems. *The International Hydrographic Review*, 30(2), 98–115.

Roshandel, S., Liu, W., Wang, C., Li, J., 2021. 3D Ocean Water Wave Surface Analysis on Airborne LiDAR Bathymetric Point Clouds. *Remote Sensing*, 13(19), 3918.

Scott, T., Austin, M., Masselink, G., Russell, P., 2016. Dynamics of rip currents associated with groynes — field measurements, modelling and implications for beach safety. *Coastal Engineering*, 107, 53–69.

Shaw, L., Helmholz, P., Belton, D., Addy, N., 2019. COMPARISON OF UAV LIDAR AND IMAGERY FOR BEACH MONITORING. *The International Archives of the Photogrammetry, Remote Sensing and Spatial Information Sciences*, XLII-2/W13, 589–596.

Sousa, P. J., Cachaço, A., Barros, F., Tavares, P. J., Moreira, P. M., Capitão, R., Neves, M. G., Franco, E., 2022. Structural monitoring of a breakwater using UAVs and photogrammetry. *Procedia Structural Integrity*, 37, 167–172.

Towards data science, 2026. Performance metrics for binary classifier. Accessed on 12 March 2026.

Tschirschwitz, F., Mechelke, K., Jansch, H., Kersten, T. P., 2016. MONITORING AND DEFORMATION ANALYSIS OF GROYNES USING TLS AT THE RIVER ELBE. *ISPRS - International Archives of the Photogrammetry, Remote Sensing and Spatial Information Sciences*, XLI-B5, 917–924.

Virshup, I., Choi, J., Lê Cao, K.-A., Wells, C. A., 2020. constclust: consistent clusters for scRNA-seq. *bioRxiv*, 2020–12.

Virtanen, P., Gommers, R., Oliphant, T. E., Haberland, M., Reddy, T., Cournapeau, D., Burovski, E., Peterson, P., Weckesser, W., Bright, J., van der Walt, S. J., Brett, M., Wilson, J., Millman, K. J., Mayorov, N., Nelson, A. R. J., Jones, E., Kern, R., Larson, E., Carey, C. J., Polat, İ., Feng, Y., Moore, E. W., VanderPlas, J., Laxalde, D., Perktold, J., Cimrman, R., Henriksen, I., Quintero, E. A., Harris, C. R., Archibald, A. M., Ribeiro, A. H., Pedregosa, F., van Mulbregt, P., SciPy 1.0 Contributors, 2020. SciPy 1.0: Fundamental Algorithms for Scientific Computing in Python. *Nature Methods*, 17, 261–272.

Wang, C., Ji, M., Wang, J., Wen, W., Li, T., Sun, Y., 2019a. An Improved DBSCAN Method for LiDAR Data Segmentation with Automatic Eps Estimation. *Sensors*, 19(1), 172.

Wang, Y., Chen, Q., Zhu, Q., Liu, L., Li, C., Zheng, D., 2019b. A Survey of Mobile Laser Scanning Applications and Key Techniques over Urban Areas. *Remote Sensing*, 11(13), 1540.

Xu, Y., Kanai, S., Date, H., Sano, T., 2022. Deep-Learning-Based Three-Dimensional Detection of Individual Wave-Dissipating Blocks from As-Built Point Clouds Measured by UAV Photogrammetry and Multibeam Echo-Sounder. *Remote Sensing*, 14(21), 5575.

Xu, Y., Yao, W., Tuttas, S., Hoegner, L., Stilla, U., 2018. Unsupervised segmentation of point clouds from buildings using hierarchical clustering based on gestalt principles. *IEEE Journal of Selected Topics in Applied Earth Observations and Remote Sensing*, 11(11), 4270–4286.

Zappia, L., Oshlack, A., 2018. Clustering trees: a visualization for evaluating clusterings at multiple resolutions. *GigaScience*, 7(7).